Available online at www.eccomasproceedia.org
Eccomas Proceedia COMPDYN (2017) 2138-2148

ECCOMAS
Proceedia

COMPDYN 2017
6th ECCOMAS Thematic Conference on
Computational Methods in Structural Dynamics and Earthquake Engineering
M. Papadrakakis, M. Fragiadakis (eds.)
Rhodes Island, Greece, 15–17 June 2017

SEISMIC RESPONSE ANALYSIS OF CONTINUOUS HIGHWAY BRIDGES UNDER NEAR-FAULT GROUND MOTIONS

Hai-Bin Ma[1], Wei-Dong Zhuo[1], Davide Lavorato[2], Gabriele Fiorentino[2], Camillo Nuti[2], Fabio Sabetta[2]

[1] Civil Engineering College, Fuzhou University
Xueyuan Road No.2 , University Town, Fuzhou City, Fujian Province
e-mail: {m140510011, zhuowd, sunying}@fzu.edu.cn

[2] Architecture Department, Roma Tre University
Largo Giovanni Battista Marzi, 10, 00153 Roma
{gabriele.fiorentino, camillo.nuti, davide.lavorato }@uniroma3.it

Keywords: Near-fault, Continuous Bridges, Time-history Analysis, Orthogonal Experimental Design, Intensify Measures

Abstract. *Ground motions in proximity to the causative fault of an earthquake are significantly affected in many cases by forward-directivity effects. The resulting seismic action on bridge is characterized by an important pulse type motion that is not considered in many international structural designed codes. In this paper, the effects of near-fault ground motions applied on regular highway bridges with design parameters selected by a sampling method, are discussed and compared with the ones of the same bridges subjected to far-fault earthquakes. Time history analyses were performed on fiber element bridge models by means of OpenSees considering seven near-fault earthquake input records with significant velocity pulse selected worldwide from the PEER database considering the same site conditions, and the El-centro earthquake record as ordinary far-field earthquake. The results are analyzed in term of top pier drift ratio, pier slenderness ratio, PGA and earthquake intensity parameters.*

Peer-review under responsibility of the organizing committee of COMPDYN 2017.
doi: 10.7712/120117.5555.18040

1 INTRODUCTION

Current design codes define seismic actions to design reinforced concrete (RC) bridges, on the base of the characteristics of the earthquakes recorded at sites distant more than 20 km from the ruptured fault (far-fault zone). However, some bridges designed in accordance with current design code but with distances minor than 20 km from the ruptured fault, have experienced severe seismic damage (1994 US Northridge, 1995 Japan Hyogoken-Nanbu, 1999 Taiwan Chi-Chi and 2008 China Wenchuan earthquake). Therefore, near-fault (NF) earthquakes can result in higher seismic demands on bridge structures which are not considered by current codes. For that reason, the definition of the proper seismic actions and the evaluation of bridge damage mechanisms in case of near-fault earthquakes should be investigated to improve the seismic design prescriptions.

NF ground motions are distinctly different from ordinary ground motions as they result short in duration, consist of one or more pulses of motions and present a significant vertical component. A literature review can help to introduce better this issue to define properly a NF action and to understand their effects on bridges.

Somerville et al. [1] reported that the near fault fault-normal forward rupture directivity velocity pulse is a narrow band pulse whose period increases with magnitude. This magnitude dependence of the pulse period causes the response spectrum to have a peak whose period increases with magnitude, so a near fault ground motions from smaller earthquakes may exceed those of larger earthquakes at intermediate periods (around 1 s).

Chopra et al. [2] concluded that the response spectrum of a near-fault earthquake record has the velocity-sensitive region narrower, and the acceleration-sensitive and displacement-sensitive regions much wider, compared to the ones of the response spectrum of a far-fault earthquake; the narrower velocity-sensitive region is shifted to longer periods.

Li et al. [3] indicated that the seismic design spectrum considering near-fault effect, especially large amplitude pulse effect of near-fault records, will significantly enhance the seismic response of continuous girder bridge.

Wang et al. [4] presented interesting elaborations of a great number of free-field ground motion records obtained during the 1999 Chi-Chi, Taiwan, earthquake. The results of these elaborations show that near fault ground motions are strongly affected by source-to-site distance, fault rupture directivity, site condition, as well as thrust of the hanging wall. Within 20 km to the causative fault, the ground motions including the duration time are much stronger than those beyond this distance.

Bozorgnia et al. [5] on the base of the characteristics of response spectra of free‐field vertical ground motion recorded during the 1994 Northridge earthquake have shown the dependence of vertical and horizontal response spectra, and their ratio, on the source-to-site distance. Verticaltohorizontal (V/H) response spectral ratio is found to be strongly dependent on period and distance. V/H spectral ratio largely exceeds the commonly assumed value of 2/3, at short periods in the nearfield region.

Saadeghvaziri et al. [6] indicated that, in general, the vertical motion will increase the level of response and the amount of damage sustained by a highway bridge.

Vertical motion generates fluctuating axial forces in the columns, which cause instability of the hysteresis loops and increase the ductility demand. Furthermore, vertical motion can generate forces of high magnitude in the abutments and foundations that are not accounted for by the current seismic design guidelines.

In this paper, the effects of near-fault ground motions applied on regular highway bridges with design parameters selected by orthogonal sampling methods, are further investigated and compared with the ones observed on the same bridges subjected to far-fault earthquakes. The characteristics of the Chinese existing RC bridges considered to perform the bridge sampling are: the bridge geometries, the steel reinforcement configurations and the material (concrete and steel characteristics) strength.

Time history analyses were performed on fiber element bridge models by means of OpenSees considering seven near-fault earthquake input records from Chi-Chi earthquake with significant velocity pulse and similar site condition selected worldwide from the PEER database considering the same site conditions, and the El Centroentro earthquake record as ordinary far-field earthquake. The results are analyzed in term of top pier drift ratio, pier slenderness ratio, PGA and earthquake intensity parameters.

1 BRIDGE SAMPLING AND MODELING

Eight Chinese highways RC bridges which have a three equal span deck with a constant section, rubber bearing and double-column pier are considered as cases of study for the present research (tab.1). In the longitudinal direction, the bridge can be characterized as SDOF system as the pier and rubber bearing contribute to the stiffness and the continuous girder contribute to the mass, while in the transverse direction, shear keys are placed on the bent cap and on the abutments to restrain transverse displacement of the superstructure as is usually done in China. The RC bridge piers were designed following capacity design rules; therefore shear failure is not expected.

The geometries and steel reinforcement configurations of these bridges were selected by an orthogonal design method on the base of the available data about the existing RC bridges in Fujian Province of China, the Chinese seismic design code [7]. The concrete and steel strength were selected by Latin Hypercube Sampling method based on the normal distribution of the most common used material in Chinese construction.

The orthogonal array used in the design is described as $L_8(2^7)$, where L is the symbol of orthogonal design, 8 is the number of experiment times, 2 is the number of factor levels and 7 the number of factors. The basic parameters of the bridge span(BS), pier slenderness ratio (PSR), longitude reinforcement ratio (LRR), transverse reinforcement ratio (TRR), longitude reinforcement strength (LRS), transverse reinforcement strength (TRS) and concrete strength (CS) for the eight representative regular bridges are shown in Tab. 1.

Bridge Number	BS (m)	PSR	LRR	TRR	LRS (MPa)	TRS (MPa)	CS (MPa)
B1	30	6	0.008	0.004	330.56	287.11	29.66
B2	30	6	0.008	0.006	341.41	308.36	30.23
B3	30	10	0.016	0.004	330.56	308.36	30.23
B4	30	10	0.016	0.006	341.41	287.11	29.66
B5	40	6	0.016	0.004	341.41	287.11	30.23
B6	40	6	0.016	0.006	330.56	308.36	29.66
B7	40	10	0.008	0.004	341.41	308.36	29.66
B8	40	10	0.008	0.006	330.56	287.11	30.23

Tab 1: Key Design parameters for the Chinese bridge sample studied; bridge span(BS), pier slenderness ratio (SR), longitude reinforcement ratio (LRR), transverse reinforcement ratio (TRR), longitude reinforcement strength (LRS), transverse reinforcement strength (TRS) and concrete strength (CS)

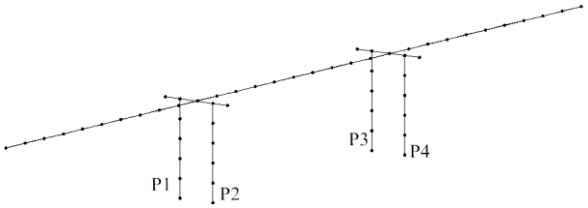

Fig 1: OpenSees bridge stick model; node configuration.

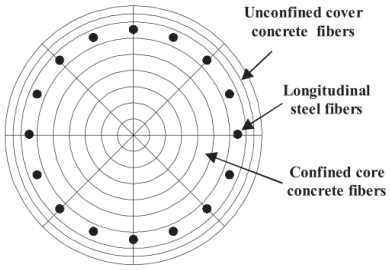

Fig 2: pier Fiber section model

The period for the bridge B1, B2,.., B8 (Tab.1) are in the range 1.0~1.6s. Each bridge was modeled by a finite element model (Fig.1) in OpenSees software [8], the bridge cap beam and the pier are modeled as fiber sections (Fig.2). As for the materials in section, Steel02 material model in OpenSees which accounts for isotropic hardening, a diminishing yield plateau and the Bauschinger effect are used to modify the steel fiber materials, Concrete02 material model which is based on the improved Kent-Park constitutive model and adjusted by Scott is used to modify the confined concrete behavior. Concrete 02 and steel02 materials were calibrated on the basis of the materials (concrete and steel) strength defined in Tab.1 for each bridge. The main property of the Concrete02 is listed as in Fig.3. Zero-Length Element with the consideration of real bearing stiffness condition is used to modify the rubber bearing on the top of the cap beam and the bridge deck is considered as the elastic case, the relevant mass is calculated based on the standard deck section drawing from Chinese Transport Ministry.

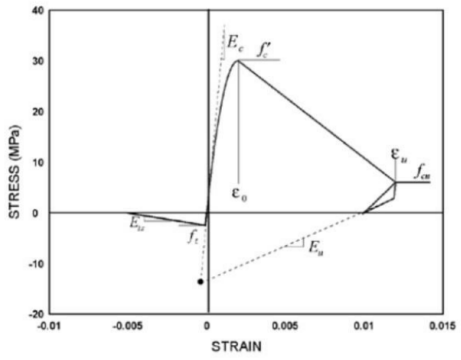

(a) Monotonic stress-strain curve of the concrete in tension and compression.

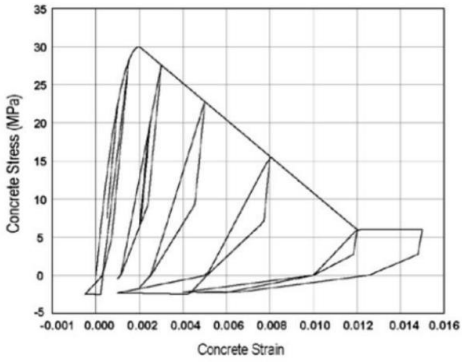

(b) Cyclic Stress-strain curve of the concrete in compression and tension

Fig 3: Concrete02 material model.

2 GROUND MOTIONS COMPARISON

Seven near fault earthquake signals (N-1,N-2,…, N-7, Fig 4 and Fig 5) which were recorded during the Chi-Chi main shock were selected from the PEER Strong Motion Database [9] to perform some time-history analysis and evaluate mean values of the bridge response according to the guidelines for seismic design of highway bridges in China [10].

Each event has fault distance (R) within 15 km and it is characterized by a significant pulse in the velocity time-history. The main parameters of these seven seismic records are given in Tab.2.

The site categories of the selected records are classified based on the average shear wave velocity to a depth of 30 m according to the Chinese seismic code: type I (V_{s30}>510 m/s), type II (260 m/s <V_{s30}≤510 m/s), type III (150 m/s <V_{s30}≤260 m/s) and type Ⅳ (Vs30≤150 m/s) [11], therefore the selected earthquake records can represent the seismic damage mechanism on site condition type II. The El Centro earthquake record is selected as the ordinary far-fault earthquake for a comparison in the next sections [10].

Number	Site Information	Fault Distance(Km)	PGA(g)	PGV(cm/s)	V_{s30}(m/s)	Pulse Period(s)
N-1	TCU068	0.32	0.60	152.61	487.34	12.29
N-2	TCU082	5.16	0.21	43.31	472.81	8.10
N-3	TCU103	6.08	0.13	62.01	494.10	8.69
N-4	TCU136	8.27	0.17	38.79	462.10	8.88
N-5	TCU056	10.48	0.14	30.91	403.20	8.94
N-6	TCU063	9.78	0.18	52.27	476.14	6.56
N-7	TCU104	12.87	0.11	27.58	410.45	7.19

Tab 2: Parameters of site condition, fault distance, PGA, PGV, V_{s30} and pulse period for the selected near-fault earthquake input.

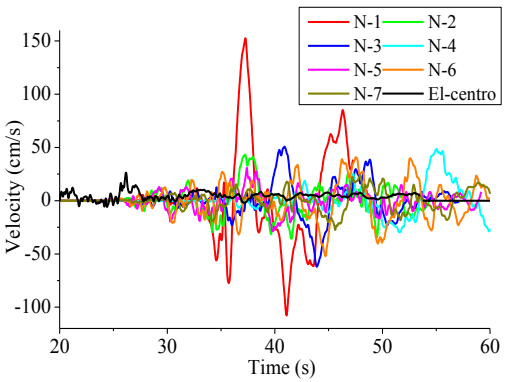

(a): The Main Velocity Pulse Component from time-history record.

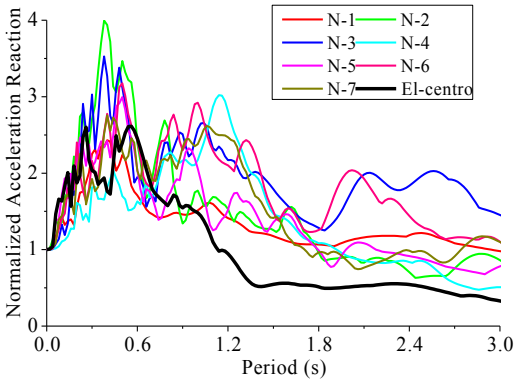

(b): The Normalized Acceleration Spectrum for inputs.

Fig.4 The Main Velocity Pulse Component and Normalized Acceleration Spectrum for the seven selected Near Fault inputs.

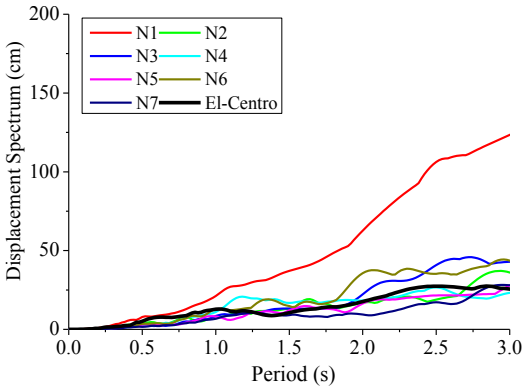

Fig 5: Displacement Spectrum for each earthquake records considered

Fig.4a and Fig.4b shows the main velocity pulse component and the normalized acceleration spectrum for the seven earthquake inputs. All the near-fault inputs present a significant velocity pulse in the range of periods 7.19~12.29s. The Normalized Acceleration Spectrum for the seven selected Near Fault inputs shows a general ascending trend with increasing periods (Fig.4b). The Near Fault seismic action can be significant due to the short transmission path as the attenuation of the earthquake energy in the near-fault region is modest. Fig.5 shows the displacement spectrum for the each earthquake records considered for time history analysis, based on the period for bridge samples ranging for 1.0~1.6s, the maximum difference at the top of the pier P1 distribute from 3.94cm to 53.30cm as elastic case.

3 RESULTS OF THE TIME HISTORY: BRIDGE DAMAGE MECHANISMS

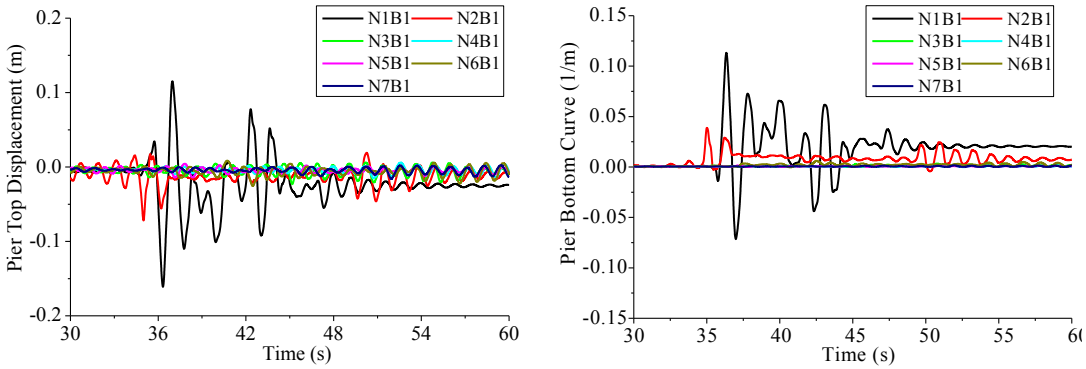

(a): Top Pier displacement history for pier P1 in longitude direction.

(b): Pier base section curvature history for pier P1 in longitude direction.

Fig.6 The time history results of top pier displacement and pier base section curvature for pier P1 in longitude direction.

The selected Near Fault seismic inputs were used to perform time history analyses with OPENSEES for each bridge model described in Tab 1.The first results of the time-history analyses are shown Fig.6a and Fig.6b in terms of top pier displacement and pier base section curvature for the longitudinal direction of pier P1 for the bridge B1 for each near-fault earthquake record. The N-1 earthquake record leads to the largest top displacement value equal to 0.115 and base section curvature value equal to 0.114.

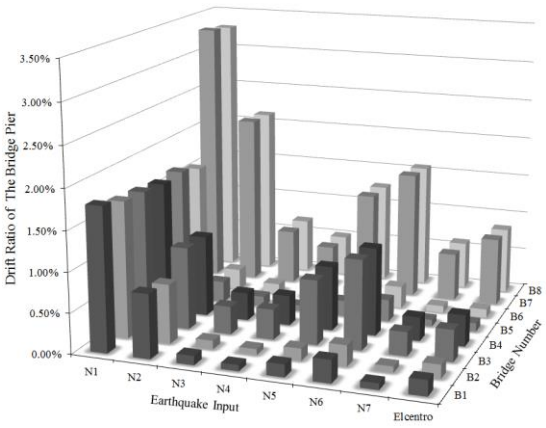

Fig 7: The Drift Ratio of the pier placed at pier P1 for each bridge considering each earthquake signals applied on the bridge.

Bridge Number	Mean-N Value	El Centro
B1	0.47%	0.19%
B2	0.44%	0.17%
B3	0.81%	0.40%
B4	0.80%	0.39%
B5	0.39%	0.11%
B6	0.37%	0.11%
B7	1.45%	0.85%
B8	1.43%	0.84%

Tab 2: The comparison between drift ratio of the pier placed at pier P1: the mean value of the drift ratio is obtained for each bridge applying each near-fault input on the bridge; the El-centro drift ratio is obtained for the same bridge by applying the El-centro earthquake

The displacement drift ratio variation depends on some pier characteristics as the slenderness ratio, axial load ratio and steel reinforcement [12] and it is a parameter which can describe the structural damage based on the pier deformation capacity. The displacement drift ratio at the top of pier, that is placed at P1 (Fig.1), is used to evaluate the structural bridge damage for different performance levels.

The drift ratio of the pier placed at pier P1 obtained applying on each bridge (B1, B2,.., B8) the seven selected Near fault seismic inputs (N1, N2,…, N7) and the El

Centro acceleration are shown in Fig.7. The maximum value (drift ratio = 1.79%) is obtained for the bridge B1 with earthquake record N1 and the minimum value (drift ration = 0.07%) is obtained in case of the bridge B4 with earthquake record N5.

Tab.2 shows the comparison between the mean value of the drift ratio obtained for each bridge by near-fault earthquakes and the drift ration obtained for the same bridge by El Centro record, the far-fault earthquake. All the mean values for the bridges under the near-fault earthquake are greater. Bridge B8 presents the maximum difference with 59% when comparing to the ordinary far-fault earthquake input.

The orthogonal experiment analysis method is selected in this study to help analyze the drift ratio of the pier and determine the level significance to each factor. There are two steps to analyze the results: range analysis and variance analysis. The range analysis assumes that when focus on the impact of one specific factor, the influence of other factors on the result is balanced. And the variance analysis is used to estimate the relative significance of each parameter in terms of contribution percentage to the overall response.

Index	BS (m)	SR	LRR	TRR	LRS (MPa)	TRS (MPa)	CS (MPa)
T_1	2.52	1.68	3.80	3.12	3.09	3.09	3.09
T_2	3.65	4.49	2.37	3.05	3.08	3.07	3.07
R_j	1.13	2.81	1.43	0.07	0.01	0.02	0.02
$\overline{x_1}$	0.63	0.42	0.95	0.78	0.77	0.77	0.77
$\overline{x_2}$	0.91	1.12	0.59	0.76	0.77	0.77	0.77
							T=6.17

Tab 6: Displacement range analytical data: summation of the data at same level, maximum difference value and the average value of summation.

Factors	*SS*	*df*	*MS*	*F*	Significance
BS (m)	0.157	1	0.157	0.783	
SR	0.994	1	0.994	4.956	**
LRR	0.252	1	0.252	1.256	
TRR	0.001	1	0.001	0.005	
LRS (MPa)	0.001	1	0.001	0.005	
TRS (MPa)	0.001	1	0.001	0.005	
CS (MPa)	0.001	1	0.001	0.005	
Deviation	1.4	7			
$F_{0.05}(1,7)=5.59$, $F_{0.1}(1,7)=3.59$, $F_{0.25}(1,7)=1.57$					

Tab 7: Drift Ratio variance analytical data: summation of the squares, freedom degree, average sum of squares and significance indicator.

This paper does not present the calculation processes of mean and range, the

details of which can be found in [13]. The results of the orthogonal experiment design calculations are summarized in Tab.6 and Tab.7 for the selected factors. In Tab.6 values of T_i, R and $\overline{x}_i$ are shown, the T_i data is obtained by summing the drift ratio of factors at the same level, R is the value for each factor calculated by finding the difference between the maximum and minimum values, $\overline{x}_i$ is the average value of T_i base on the calculation time and the T is the summation of all values. For example, if levels for focused factor is assumed as A and B, for each factor in $L_8(2^7)$ the calculation time is 4, then the $\overline{x}_i$ value can be calculated as Eq 1.

$$\overline{x}_i = (A_1+A_2+A_3+A_4)/4 \tag{1}$$

Tab.7 presents the sum of squares, degrees of freedom, F variance ratio, F standard value and the significance where SS represent the summation of the squares, df represent the degree of freedom, MS represent the average sum of squares and F represent the significance indicator [13]. The F standard value is determined from an F-table for a given statistical level of significance. If the F variance ratio ranks higher than the F standard value, the corresponding factor will have significant contributions to the overall results. The tables for various significance levels and different degrees of freedom are available in most handbooks [14].

The range and variance analysis about the pier drift ratio show that the slenderness ratio of the pier is the most significant factor where significant indicates values larger than F distribution at α=0.1. The longitudinal reinforcement ratio is the second significant factor with an F value larger than the F distribution at α=0.25.

4 DAMAGE PARAMETER COMPARISON

Previous research results showed that the drift ratio of the pier and the earthquake intensify measure parameter follow a linear distribution in the natural logarithmic coordinate system [15].

The relationship between the response of the bridge, for example the pier drift ratio D obtained by time history analysis, and a parameter IM, that gives information about the characteristics of the input record used for the analyses can be described by Eq.1. The record parameter can be the PGA, PGV, Housner Intensity, PGV×Tp, the ratio PGV/PGA and the ratio PGD/PGV where the PGA is the peak ground acceleration, PGV is the peak ground velocity, PGD is the peak ground displacement, Housner Intensity is a parameter which reflects the response spectrum intensity [16] and PGV×Tp represents the impulse intensity [17]. The coefficients (a, b) of this equation can be calibrated by means of a regression analysis of the time history analysis results of the bridge B1. The record parameters considered are:

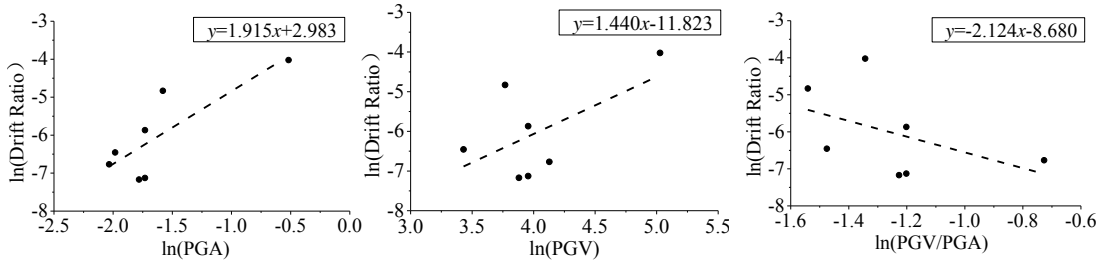

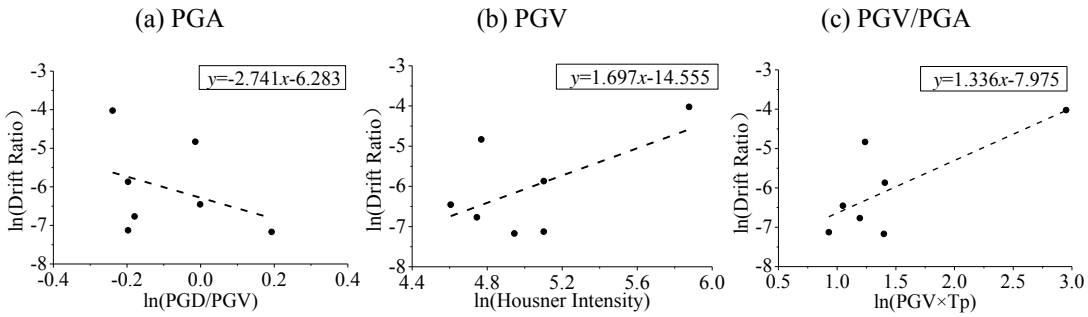

Fig 8: Relationship between the drift ratio D and different IM parameter on the base of the results of the nonlinear analyses on bridge B1.

$$\ln D = a \ln(IM) + b \tag{2}$$

The results of the Eq 2 calibration are shown in Fig.8: the PGA, PGV, Housner Intensity and PGA×T_p have a positive correlation with the bridge drift ratio D whereas the PGV/PGA and PGD/PGV show a negative correlation with the bridge drift ratio D. The Fig.8 shows that the PGA factor is the most correlated parameter for the bridge drift ratio D as it shows the minimum residual sum of square value.

5 CONCLUSION

This paper compared the seismic response of Chinese RC bridge subjected to near-fault earthquake or far fault earthquakes recorded on the same site type. The results of this study demonstrate that:

- When compared with ordinary far-fault earthquake, the near-fault earthquake shows higher velocities component during the time history and higher acceleration spectrum value for long periods.
- The mean values of the bridge pier drift ratio for different bridge samples are all greater than the ones evaluated in case of ordinary far-fault earthquake; the slenderness ratio is the most significant factor for the seismic response according to orthogonal analysis result.
- Based on the selected earthquake records, the PGA have the most related correlation with the bridge pier drift ratio.

Ongoing work is focused on expanding the sample coverage of both earthquake records and the bridge samples.

REFERENCES

[1] Somerville, P. G., 2002, Characterizing Near-Fault Ground Motion for the Design and Evaluation of Bridges, *Proceedings of Third National Seismic Conference and Workshop on Bridges and Highways*, Portland, USA, 2002, Apr. 29-May 1.

[2] Chopra, A. K., and Chintanapakdee, C., Comparing Response of SDOF

Systems to Near-Fault and Far-Fault Earthquake Motions in the Context of Spectral Regions, *Earthquake Engineering and Structural Dynamics*, 2001,30(12): 1769-1789.

[3] Li X, Jiang H, Dan S. Study on Seismic Safety Performance for Continuous Girder Bridge based on Near-fault Strong Ground Motions. *Procedia Engineering*, 2012, 45(2):916-922.

[4] Wang, G. Q., Zhou, X. Y., Zhang, P. Z. & IGEL, H. 2002. Characteristics of amplitude and duration for near fault strong ground motion from the 1999 Chi-Chi, Taiwan Earthquake. *Soil Dynamics and Earthquake Engineering*, 2002, 22(1): 73-96.

[5] Bozorgnia Y, Niazi M and Campbell KW (1995), Characteristics of free-field vertical ground motion during the Northridge earthquake, E*arthquake Spectra*, 1995, 11 (4): 515–525.

[6] Saadeghvariri M A, Foutch D A. Dynamic behaviour of R/C highway bridges under the combined effect of vertical and horizontal earthquake motions. *Earthquake Engineering & Structural Dynamics*, 1991, 20(6):535-549.

[7] JTG/T B02-01-2008. Guidelines for seismic design of highway bridges. Beijing: People's Communications Press. (in Chinese)

[8] OPENSEES. Open system for earthquake engineering simulation. 2009, http://opensees. berkeley.edu.

[9] PEER, available from URL: http://peer.berkeley.edu/smcat/search.html. Accessed December 2013.

[10] Guidelines for Seismic Design of Highway Bridge. Beijing: China Communication Press, 2008.(in Chinese)

[11] Lv HS, Zhao FX. Site coefficients suitable to China site category. Earthquake Science, 2007, 20(1):71-79. (in Chinese).

[12] Shome N. Probabilistic seismic demand analysis of nonlinear structures, Ph.D. Thesis, Department of Civil and Environmental Engineering, Stanford University, Stanford, 1999.

[13] Wirier BJ, Brown DR, Michels KM. Statistical principles in experimental design. New York: McGraw-Hill: 1971.

[14] Cogkun S, Motorcu AR, Yamankaradeniz N, Pulat G. Evaluation of control parameters' effects on system performance with Taguchi method in waste heat recovery application using mechanical heat pump. Int J Refrig 2012;35(4):795-809.

[15] Ma H B, Zhuo W D, Yin G, et al. A Probabilistic Seismic Demand Model for Regular Highway Bridges. *Applied Mechanics & Materials*, 2016, 847:307-318.

[16] Housner G W. Limited Design of structures to Reisist Earthquake. *Proc. 1st world conf. Earthquake Eng*. Berkeley, California, 1956. 5-13.

[17] Jiang H, Zhu X. Velocity Pulse Effects of Near-fault Earthquakes and Isolation Characteristic of Continuous Girder Bridges. *China Safety Science Journal*, 2003; 13(12):57-62.